Journal of Magnetism and Magnetic Materials 596 (2024) 171922

Contents lists available at ScienceDirect

Journal of Magnetism and Magnetic Materials

journal homepage: www.elsevier.com/locate/jmmm

Research article

Out-of-equilibrium voltage and thermal bias response of a quantum dot hybrid system coupled to topological superconductor

Piotr Trocha [a,b,*], Thibaut Jonckheere [b], Jérôme Rech [b], Thierry Martin [b]

[a] Institute of Spintronics and Quantum Information, Faculty of Physics, Adam Mickiewicz University, 61-614, Poznań, Poland
[b] Aix Marseille Univ., Université de Toulon, CNRS, CPT, Marseille, France

ARTICLE INFO

Keywords:
Quantum dot
Majorana fermions
Topological superconductor
Nonequilibrium transport
Thermocurrent

ABSTRACT

We investigate theoretically the out-of-equilibrium transport properties of a single-level quantum dot coupled to a normal metal electrode and attached to a topological superconductor. Both voltage and thermal bias responses of the system in the nonequilibrium regime are studied. To obtain transport characteristics we used the nonequilibrium Green's function approach. Particularly, we calculated the current and the corresponding differential conductance in two distinct cases. In the former situation, the charge current is induced by applying a bias voltage, whereas in the latter case it is generated by setting a temperature difference between the leads with no bias voltage. Moreover, strong diode effect in thermally generated current is found and non-equilibrium thermopower is analyzed.

1. Introduction

Discovery of Majorana bound states (MBSs) in a topological nanowire [1–3] has initiated investigations on the transport properties of hybrid systems, especially those including quantum dots [4,5]. Most studies have been devoted to the systems in which the topological superconductor has been described by low energy limit including only MBSs, whereas the above-gap quasiparticle bands have been disregarded. Such models are not sufficient to correctly describe the thermoelectric properties of a hybrid system consisting of normal metal and topological superconducting leads. Due to particle-hole symmetry MBSs do not contribute to the thermoelectric response resulting in a vanishing Seebeck coefficient (thermopower) [6]. Thus, most investigations have focused on the influence of the MBS on the thermoelectric response in systems in which a temperature difference has been set between two normal metal leads [7–20]. In turn, here we investigate a two-terminal system consisting of a single-level quantum dot coupled to a normal metal electrode and a topological superconductor which includes not only MBS but also the quasiparticle states at energies beyond the gap. These quasiparticle states lead to a nontrivial thermoelectric response of the considered system in which subgap states may only indirectly influence it to some extent. It is worth noting that the thermoelectric properties of QD's hybrid systems with topological superconductor described within finite gap models are greatly unexplored [21].

The paper is organized in the following way. In Section 2 we present the theoretical description of the considered system. Particularly, we introduce the model taken into consideration and derive the formulas for the current and the corresponding differential conductance. The numerical results are presented and discussed in Section 3. Finally, the paper is concluded in Section 4.

2. Theoretical framework

The system taken into consideration consists of a single-level quantum dot coupled to a normal metal (NM) and a topological superconductor (TS) which is described by the Hamiltonian of the following form;

$$H = H_{NM} + H_{TS} + H_{QD} + H_{T_{NM}} + H_{T_{TS}}. \tag{1}$$

The first term, H_{NM}, describes a normal metal electrode and acquires the form, $H_{NM} = \sum_{\mathbf{k}} \varepsilon_{\mathbf{k}} c^{\dagger}_{\mathbf{k}NM} c_{\mathbf{k}NM}$ with $\varepsilon_{\mathbf{k}}$ denoting electron energy of the state with wave vector $\mathbf{k}$. Here, we consider spinless electrons, as it is required to apply strong magnetic field to form Majorana modes. This assumption is consistent with the experimental realization of Majorana bound states in a semiconductor nanowire with strong spin–orbit interaction deposited on s-wave superconductor and in the presence of strong magnetic field [1–3]. The same formulation has been adopted in [5–7]. Generally, the NM lead can be magnetic but as long as only electrons with one spin orientation couple to the TS we can

* Corresponding author at: Institute of Spintronics and Quantum Information, Faculty of Physics, Adam Mickiewicz University, 61-614, Poznań, Poland.
E-mail address: ptrocha@amu.edu.pl (P. Trocha).

https://doi.org/10.1016/j.jmmm.2024.171922
Received 15 September 2023; Received in revised form 25 February 2024; Accepted 6 March 2024
Available online 7 March 2024

disregard the other one and omit the spin index. The corresponding retarded/advanced Green's function acquires the form in Nambu space, $\mathbf{g}^{r/a}_{NM} = \mp i\pi\rho_{NM}\sigma_0$ with ρ_{NM} denoting the density of states of the normal metal reservoir. In turn, H_{TS} stands for the Hamiltonian of the TS lead described by the low-energy limit of a Kitaev chain [22];

$$H_{TS} = \int_0^\infty dx \Psi^\dagger_{TS}(x)(-iv_F\partial_x\sigma_z + \Delta\sigma_y)\Psi_{TS}(x). \tag{2}$$

Here, we assume the proximity-induced gap as real positive and $\Psi_{TS} = (c_r, c_l^\dagger)^T$ is a Nambu spinor with right- and left-moving fermion operators. The relevant boundary retarded/advanced Green's function acquires the following form [22];

$$\mathbf{g}^{r/a}_{TS}(\omega) = \pi\rho_N \frac{[\theta(\Delta-|\omega|)\sqrt{\Delta^2-\omega^2} \mp i\ \mathrm{sgn}(\omega)\theta(|\omega|-\Delta)\sqrt{\omega^2-\Delta^2}]\sigma_0 + \Delta\sigma_x}{\omega \pm i0^+} \tag{3}$$

with ρ_N being the density of states in the normal state. The corresponding density of states has the form;

$$\rho_{TS}(\omega) = \pi\rho_N\left[\frac{\theta(|\omega|-\Delta)\sqrt{\omega^2-\Delta^2}}{\pi|\omega|} + \Delta\delta(\omega)\right] \tag{4}$$

which clearly states that the zero-energy Majorana bound state is the intrinsic feature of the topological superconductor. Above, σ_x denotes a relevant Pauli matrix, whereas σ_0 is a unit matrix of the same dimension.

The quantum dot is modeled by a Hamiltonian of the following form;

$$H_{QD} = \varepsilon_d d^\dagger d \tag{5}$$

with ε_d denoting the dot's energy level. The last two terms of the Hamiltonian (1) describe tunneling of electrons between the dot and the leads and acquire the following form;

$$H_{T_{NM}} = \sum_{\mathbf{k}}(V_{NM}c^\dagger_{\mathbf{k}}d + \mathrm{H.c.}), \tag{6}$$

for coupling to the normal metal lead, and

$$H_{T_{TS}} = V_{TS}\psi^\dagger_{TS}(0)d + \mathrm{H.c.}, \tag{7}$$

for coupling to the TS lead. Here, we assumed independent wave vector tunneling matrix elements V_i for $i = NM, TS$. Furthermore, we parametrize the coupling of the dot to ith lead by $\Gamma_i = 2\pi|V_i|^2\rho_i$ with ρ_i being the density of states in the ith lead in the normal state. In the superconducting (SC) state the coupling becomes modified for the TS electrode.

The coupling matrix in the Nambu space can be represented in matrix form,

$$\mathbf{V}_i = V_i\sigma_z, \tag{8}$$

whereas the corresponding retarded/advanced self-energies one can find using,

$$\mathbf{\Sigma}^{r/a}_i = \mathbf{V}^\dagger_i\mathbf{g}^{r/a}_i\mathbf{V}_i \tag{9}$$

where $\mathbf{g}^{r/a}_i$ is the retarded/advanced Green function for the ith lead defined above. Then, the coupling matrix $\mathbf{\Gamma}_i$ (for $i = NM, TS$) is expressed by,

$$\mathbf{\Gamma}_i = i[\mathbf{\Sigma}^r_i - \mathbf{\Sigma}^a_i] \tag{10}$$

The full retarded/advanced Green's function of the coupled dot $\mathbf{G}^{r/a}_d$ is obtained from the Dyson equation,

$$\mathbf{G}^{r/a}_d = [(\mathbf{g}^{r/a}_d)^{-1} - \mathbf{\Sigma}^{r/a}]^{-1}, \tag{11}$$

with $\mathbf{g}^{r/a}_d$ denoting the bare dot's retarded/advanced Green's function in Nambu space, $[\mathbf{g}^{r/a}_d]^{-1} = \mathrm{diag}(\omega - \varepsilon_d \pm i0^+, \omega + \varepsilon_d \pm i0^+)$, and $\mathbf{\Sigma}^r = \mathbf{\Sigma}^r_{NM} + \mathbf{\Sigma}^r_{TS}$. In the wide band approximation and using Eq. (9) one obtains the self-energy for the dot's coupling $\mathbf{\Sigma}^r_{NM} = -\frac{i}{2}\Gamma_{NM}\sigma_0$ to the NM lead and $\mathbf{\Sigma}^r_{TS} = \frac{\Gamma_{TS}}{2\pi\rho_N}\sigma_z\mathbf{g}^r_{TS}\sigma_z$ to the TS reservoir.

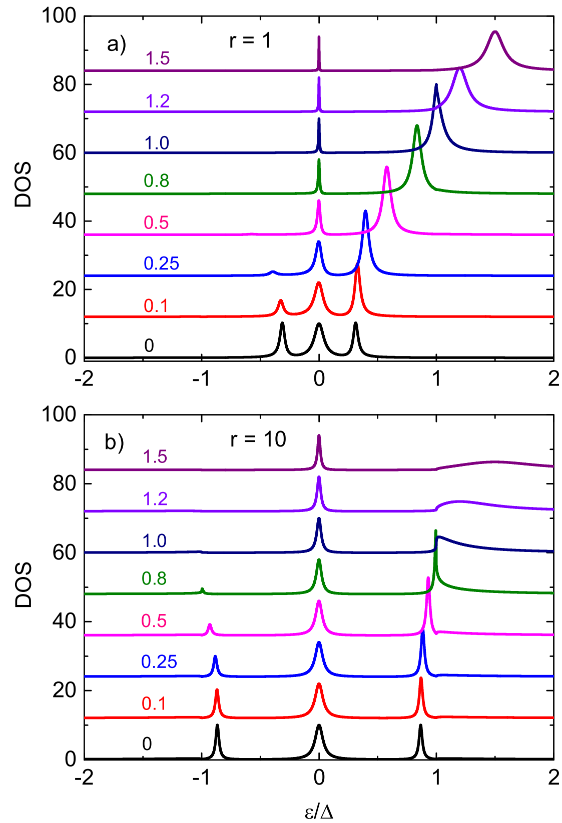

Fig. 1. Zero-temperature density of states for the quantum dot calculated for indicated values of dot's energy level, ε_d/Δ, and for coupling asymmetry parameter (a) $r = 1$, (b) $r = 10$. The other parameters are: $\Gamma = 0.1\Delta$.

To calculate the charge current we employ the non-equilibrium Green's function technique. Following Ref. [23], one can show that the charge current flowing through NM junction is expressed by;

$$J_e \equiv J^e_{NM} = \frac{e}{h}\int d\varepsilon \Big[(f_{\omega-\mu_{NM}} - f_{\omega+\mu_{NM}})\mathcal{T}_A(\omega) + (f_{\omega-\mu_{NM}} - f_{\omega-\mu_{TS}})\mathcal{T}_S(\omega)\Big], \tag{12}$$

with $\mathcal{T}_A(\omega) = G^r_{12}[\boldsymbol{\Gamma}_{NM}\boldsymbol{G}^a\boldsymbol{\Gamma}_{NM}]_{21} = \Gamma^2_{NM}|G^r_{12}|^2$, $\mathcal{T}_S(\omega) = [\boldsymbol{G}^r\boldsymbol{\Gamma}_{TS}\boldsymbol{G}^a\boldsymbol{\Gamma}_{NM}]_{11}$. Here, $f_{\omega-\mu_i} = \{\exp[(\omega-\mu_i)/k_BT_i] + 1\}^{-1}$ is the Fermi-Dirac distribution function for the lead i with μ_i and T_i denoting the corresponding chemical potential and temperature, while k_B stands for the Boltzmann constant. We relate the chemical potential of the NM lead to the voltage V as $\mu_{NM} = eV$, assuming the TS electrode is grounded, $\mu_{TS} = 0$. Temperature is measured with respect to the TS lead, i. e. $T_{TS} = T$ and $T_{NM} = T + \delta T$. For completeness, the current flowing through the TS junction is obtained from particle (charge) conservation, $J_{TS} = -J_{NM} = -J_e$. Moreover, we assume that the bare energy level of the dot is independent of the applied bias voltage. This can be achieved for instance with a suitable gate voltage which tunes the dot's energy level.

3. Numerical results

We approximate the temperature dependence of the superconducting gap by the formula $\Delta(T) = \Delta\sqrt{1-(T/T_c)^3}$ with Δ denoting the energy gap at zero temperature, whereas T_c is the critical temperature at which superconductivity vanishes. Furthermore, for a topological nanowire one can assume $\Delta = 1.764k_BT_c$ [24].

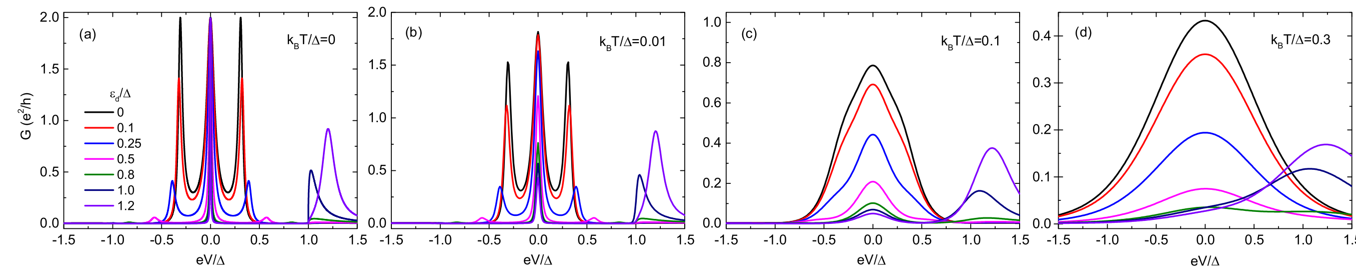

Fig. 2. Differential conductance as a function of bias voltage calculated for indicated values of dot's energy level and for (a) $k_BT = 0$, (b) $k_BT = 0.01\Delta$, (c) $k_BT = 0.1\Delta$, (d) $k_BT = 0.3$. The other parameters are: $\Gamma_{NM} = \Gamma_{TS} = 0.1\Delta$, $\delta T = 0$.

Generally, we assume an asymmetry in the coupling strengths of the QD to NM and TS leads introducing the parameter r parametrizing the relevant couplings by $\Gamma_{NM} = \Gamma$ and $\Gamma_{TS} = r\Gamma$. In the numerical calculations we express all energy quantities in the units of zero temperature superconducting gap energy, Δ and assume that $\Gamma = 0.1\Delta$.

In this section we present the numerical results on electrically and thermally induced charge transport in the considered system. However, to get deeper insight into presented results, let us first consider the local density of states of a quantum dot coupled to the external electrodes. In Fig. 1 we present the local density of states calculated for different values of the dot's energy level and for (a) symmetric ($r = 1$) and (b) highly asymmetric ($r = 10$) couplings. For dot's energy level $\varepsilon_d = 0$ the density of states reveals a symmetric (with respect to the zero energy) three-peak structure, consisting of one central resonance and two side maxima, regardless of the coupling strength to the TS electrode. Moreover, all three peaks acquire equal amplitude for $\varepsilon_d = 0$. However, the satellite peaks move away from the central maximum when the coupling strength to the TS increases. When the dot's energy level moves away from zero, one of the side peaks of the DOS becomes more pronounced, whereas the other one gradually disappears and vanishes for $\varepsilon_d \approx 0.5\Delta$ and $r = 1$ ($\varepsilon_d \approx \Delta$ and $r = 10$). This means that in this case the satellite peaks cease to participate in transport as Andreev processes require both of them. Meanwhile, the intensity and position of the central peak is immune to the change in both the dot's energy level and the asymmetry in couplings, which clearly states that one deals with a MBS state. Apart from that, the width of the central peak in the DOS becomes more and more narrow with increasing dot's energy level regardless of the coupling strength to the TS electrode, indicating that the MBS becomes more and more localized at zero energy. However, this tendency is more pronounced for the symmetric case ($r = 1$) than for much larger dot's coupling to TS ($r = 10$). In turn, for $\varepsilon_d/\Delta \geq 1$ (or $\varepsilon_d/\Delta \leq -1$) finite features appear in the above-gap region, associated with quasiparticle tunneling.

Now, we consider the bias voltage dependence of the charge current and the corresponding differential conductance. The differential conductance, G, is defined as the derivative of the electrical current with respect to the applied bias voltage under zero temperature difference;

$$G = \left.\frac{\mathrm{d}J_e}{\mathrm{d}V}\right|_{\delta T=0}. \tag{13}$$

Analyzing Eq. (12) one can notice that both sub-gap and above-gap states contribute to G. In Fig. 2 we present the differential conductance as a function of bias voltage calculated for indicated values of the dot's energy level and for various temperatures. Specifically, in Fig. 2(a) zero temperature bias voltage dependence of G is displayed. Generally, the differential conductance in the sub-gap regime consists of three peaks. Regardless of the dot's level position, the differential conductance reveals a zero bias peak (ZBP) of maximal allowed intensity, i. e. two quanta of conductance $2e^2/h$. On the other hand, intensities of the side peaks achieve maximal values only for $\varepsilon_d = 0$ and rapidly diminish as the dot's level position moves away from zero. We must point out that the present situation differs substantially from the case in which the TS electrode is replaced by an *s-wave* superconducting lead. In the latter system, the sub-gap differential conductance reveals one- or two-peak structure depending on the coupling strength to the SC reservoir and/or the position of the dot's level [25]. This allows to distinguish the two systems. The zero bias peak is directly related to the Majorana zero mode, whereas the side peaks come from energy-level splitting caused by the coupling to the TS. We note that a ZBP has been experimentally observed in hybrid topological nanowire devices [1–3]. The broadening of the central and side peaks originates from the coupling to the NM reservoir. The position of the ZBP is pinned at zero bias voltage for any dot's level which results from particle-hole symmetry. This feature in G differs from that revealed in a QD coupled to normal metal and *s-wave* superconductor in which the zero bias conductance diminishes when tuning the dot's energy level away from zero [26,27]. Moreover, the width of the ZBP decreases when tuning the dot's energy level away from $\varepsilon_d = 0$ and for sufficiently large $\varepsilon_d \gg \Delta$, i. e. for $\varepsilon_d \to \infty$, it tends to zero.

When the dot's level position is close to the superconducting gap edge, the above-gap conductance becomes relevant because quasiparticle tunneling is allowed. Even for $\varepsilon_d \ll \Delta$ the above-gap conductance exists but is obscured due to the relatively large intensity of the sub-gap conductance. In turn, for $\varepsilon_d \gtrsim \Delta$ the conductance at $eV > \Delta$ becomes significant. A similar situation emerges when the dot's energy level is negative with the difference that the over-gap feature appears for $eV < -\Delta$.

So far, we have considered the zero temperature limit but as we will see, finite temperature has a profound influence on the differential conductance. Interestingly, a relatively small change in temperature significantly influences the differential conductance, especially in the sup-gap region. Both the intensity of the ZBP and the side-peaks become reduced when a finite temperature is switched on. Surprisingly, the intensity of the ZBP drops further down when moving the dot's energy level away from zero. The former feature is due to the smoothening of the Fermi-Dirac distribution with temperature. It results in a smaller density of electrons (holes) around eV ($-eV$) (as they are redistributed in a broader range of energies) and as a consequence leads to a slower rise of the current when tuning the bias voltage. The aforementioned temperature dependence of the Fermi-Dirac function together with the behavior of the MBS peak's width when tuning the dot's energy level explains this latter feature.

For sufficiently large temperatures ($k_BT > 0.05\Delta$) the three-peak structure of the differential conductance merges into a single resonance, whose width increases with rising temperature. Simultaneously, the intensity of the peak decreases. Similar behavior reveals the above-gap feature resulting from quasiparticle tunneling. Generally, when the temperature is relatively large and for detuning of the dot's level outside of the superconducting gap, the quasiparticle contribution to G surpasses the sub-gap one.

Now, we consider the generation of charge current by means of a temperature difference set between the NM and TS leads and assuming

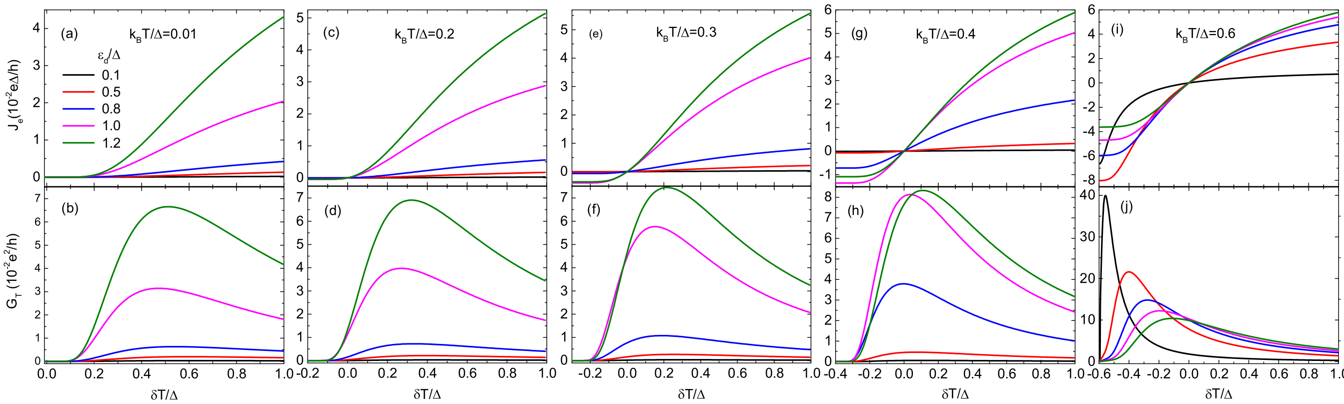

Fig. 3. Thermocurrent (upper panel) and differential conductance (lower panel) as a function bias temperature calculated for indicated values of dot's level energy and for (a)–(b) $k_BT = 0.01\Delta$, (c)–(d) $k_BT = 0.05\Delta$, (e)–(f) $k_BT = 0.1\Delta$, (g)–(h) $k_BT = 0.2\Delta$, (i)–(j) $k_BT = 0.3\Delta$, (k)–(l) $k_BT = 0.4\Delta$, (m)–(n) $k_BT = 0.6\Delta$. The other parameters are: $\Gamma_{NM} = \Gamma_{TS} = 0.1\Delta$, $V = 0$.

zero bias voltage $V = 0$. Such current is called thermocurrent and the corresponding thermoconductance is defined as;

$$G_T = \left.\frac{\mathrm{d}J_e}{\mathrm{d}T}\right|_{V=0}. \tag{14}$$

In Fig. 3 we present thermocurrent and the corresponding thermoconductance, G_T, as a function of the applied temperature bias δT calculated for indicated values of the dot's energy level and for different temperatures T. First of all, when the temperature bias is zero, no current flows through the system. One can notice that, for low temperature and relatively small temperature bias δT, the current is strongly suppressed for both positive and negative temperature bias. We remind that temperature bias is applied only to the normal metal lead, i. e. $T_{NM} = T + \delta T$. For low T, there is a small number of quasiparticles which can tunnel to the normal electrode when negative bias temperature is set. On the other hand, for positive but small δT there are not enough high energetic electrons in the normal lead that can be transferred to the TS reservoir. However, increasing the temperature bias, and thus, the temperature of the NM lead, the number of high energetic electrons grow and the current starts to flow. Of course, when the dot's energy level is deep in the SC gap this current is relatively small but rises when ε_d reaches the edges of the SC gap and becomes significant for $|\varepsilon_d| \geq \Delta$. When ε_d is located deep in the SC gap, the high energetic electrons from the normal electrode can be transferred to the TS's quasiparticle states only via the tails of the dot's level, whereas for $|\varepsilon_d| \geq \Delta$ the electrons can tunnel resonantly through the dot. Regardless of the dot's level position, the thermocurrent monotonically grows with increasing δT. The corresponding thermoconductance strictly follows the behavior of the current: it acquires small values for ε_d deep inside the SC gap and becomes relatively large for $|\varepsilon_d| \geq \Delta$. The location of the maximum of the thermoconductance moves towards lower values of δT with increasing temperature T (and for $k_BT < \Delta$).

When the temperature T is sufficiently high, more electrons can be excited to the quasiparticle states and the thermocurrent at negative temperature bias becomes relevant, especially for $|\varepsilon_d| \geq \Delta$ as shown in Figs. 3(e) and in 3(g). However, the thermocurrent for negative δT and the one for the corresponding positive δT still differ significantly. This asymmetry in the thermocurrent with respect to the temperature bias reversal leads to a rectifying effect. The negative δT bias does not influence the number of quasiparticles in the TS, whereas a positive δT increases the population of high energetic electrons in the NM lead which can be transferred to the TS reservoir. This explains the resulting asymmetry in the current. Generally, both the thermocurrent (in the sense of its absolute value) and the corresponding thermoconductance grow with increasing temperature. However, for sufficiently high temperature an exception occurs for $|\varepsilon_d| \geq \Delta$ [see Fig. 3(g)]. In this case, the absolute value of the current and the corresponding thermoconductance acquire larger values for smaller ε_d at negative temperature bias. The larger the dot's level value, the higher energetic electrons are able to be transferred through the dot, but their population becomes reduced due to the Fermi-Dirac distribution temperature dependence. Consequentially, smaller thermocurrent flows for larger ε_d at sufficiently high temperature. We point out that in general, this effect is present independently of temperature but requires a sufficiently large value of the dot's level i. e. the smaller the temperature the larger the value of ε_d to consider. However, due to the temperature dependence of the superconducting gap, which becomes smaller as the temperature rises and specifically for $k_BT = 0.4\Delta$, $\Delta(T = 0.4\Delta/k_B) \approx 0.8\Delta$, one can observe this phenomenon for $\varepsilon_d/\Delta = 1.2$.

Apart from that, the J and G_T for $\varepsilon_d = 0.8\Delta$ seem to be much larger in comparison with those noticed at lower T which is also a consequence of the temperature dependence of the SC gap. This is not surprising, as $\Delta(T = 0.4\Delta/k_B) \approx 0.8\Delta$.

To compare the results obtained for the topological phase, we also calculated the thermocurrent and the corresponding thermoconductance for a temperature above the critical value, $T > T_c$, presented in Fig. 3(i-j). Thus, the SC gap is closed and the TS reservoir is in the normal state. Due to the lack of an energy gap, significant current can flow for $|\varepsilon_d| \ll \Delta$. Of course, both in the topological phase and in the normal state, the thermocurrent vanishes for $\varepsilon_d = 0$ due to bipolar effect i. e. the thermally induced current carried by electrons is compensated for by the current due to holes. One can notice that the thermocurrent in topological and in normal phase behaves differently for negative thermal bias. In turn, thermoconductance acquires maximal values for negative temperature bias oppositely to those in the topological phase. Moreover, in the normal phase it decreases with increasing dot's energy level.

Here, we presented results for positive dot's energy level, $\varepsilon_d > 0$. However, due to symmetry, the corresponding results for $\varepsilon_d < 0$ can be obtained making the transformation: $\varepsilon_d \to -\varepsilon_d$ then $J_e \to -J_e$ and $G_T \to -G_T$.

Better visualization of the diode effect associated with thermally generated current can be achieved by introducing a rectification factor quantified by the ratio [28]

$$R = \frac{|J_e^+| - |J_e^-|}{|J_e^+| + |J_e^-|} \tag{15}$$

with J_e^+ being calculated for $\delta T > 0$, whereas J_e^- has been obtained for the corresponding negative temperature bias, $\delta T < 0$. According to the above definition, there are no rectification for $R = 0$ and the thermocurrent is maximally rectified for $R = 1$ or $R = -1$. Thus, the former situation corresponds to $|J_e^+/J_e^-| = 1$, whereas the latter case occurs when $J_e^- = 0$ or $J_e^+ = 0$ and the other current being finite, i. e. J_e^+ or J_e^-, respectively. The definition given by Eq. (15) has an important

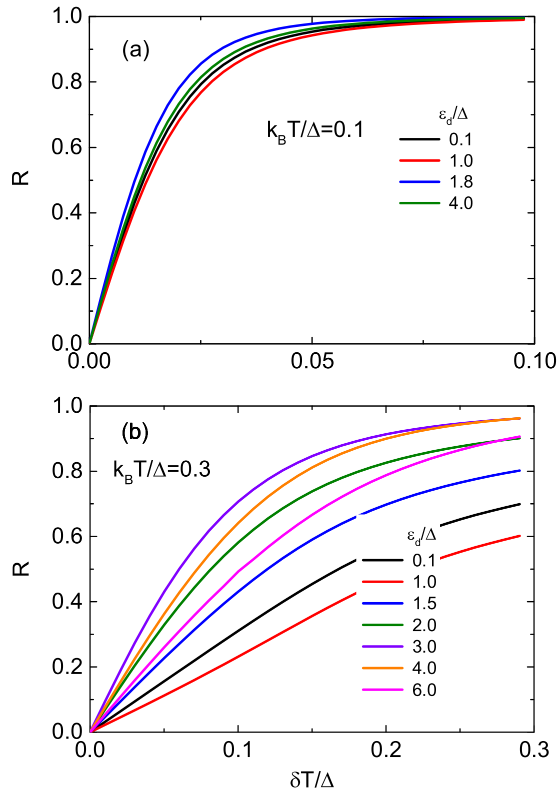

Fig. 4. Rectification ratio as a function of bias temperature calculated for indicated values of dot's level energy and for (a) $k_BT = 0.1\Delta$, (b) $k_BT = 0.3\Delta$. The other parameters are: $\Gamma_{NM} = \Gamma_{TS} = 0.1\Delta$, $V = 0$.

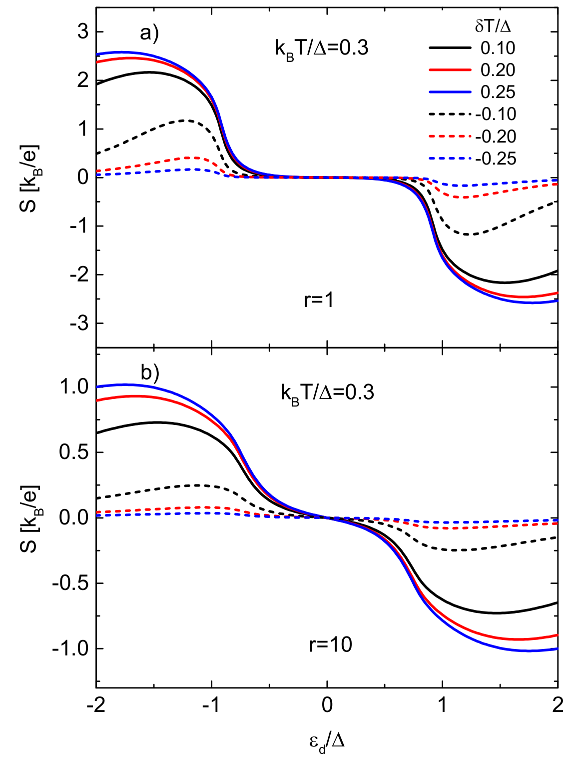

Fig. 5. Non-equilibrium Seebeck coefficient as a function of the dot's energy level calculated for indicated values of temperature bias, and for (a) $r = 1$, (b) $r = 10$. The other parameters are: $k_BT = 0.3\Delta$ $\Gamma_{NM} = 0.1\Delta$, $V = 0$.

advantage over the commonly used rectification ratio ($|J_e^+/J_e^-|$) as it results in better resolution of the curves calculated for different values of a given parameter [28,29]. In Fig. 4 the rectification ratio is shown for the indicated values of dot's energy level and for two different temperatures of the TS electrode. Note that by tuning δT, only the temperature of the normal lead, T_{NM}, is changed leaving T_{TS} constant.

The ratio R grows monotonically with increasing temperature difference, δT, regardless of the temperature of the TS electrode. This rise is strictly related with the current dependence on $\pm\delta T$ described above. Particularly, for lower temperature of the TS lead, the R factor grows faster with δT reaching the maximal value of one. In turn, the dot's energy level dependence of the rectification factor R is nonmonotonic. Firstly, R drops with increasing ε_d from $\varepsilon_d \approx 0$ to $\varepsilon_d/\Delta \approx 1$. Then, for $\varepsilon_d/\Delta > 1$ it grows, reaching its maximal value for ε_d^{max} (which depends on the temperature of the TS electrode), and decreases with further increasing ε_d. Surprisingly, the lowest rectification is noted for $\varepsilon_d = \Delta$. The rise in R in the range of $\varepsilon_d \in (\Delta, \varepsilon_d^{max})$ can be understood as follows. Thermocurrent J_e^+ grows with increasing ε_d up to $\varepsilon_d/\Delta \approx 1.2$ and then drops. The rise is due to the fact that around $\varepsilon_d/\Delta \approx 1.2$ the whole width of the dot's level becomes available for quasiparticle tunneling. However, with further increase in ε_d, less electrons can be transferred from NM to TS lead and J_e^+ drops. On the other hand, $|J_e^-|$ monotonically decreases with increasing ε_d as the number of available quasiparticles that can tunnel to NM lead also decreases. However, up to $\varepsilon_d/\Delta = \varepsilon_d^{max}$, the rate of drop of $|J_e^-|$ is faster than that of $|J_e^+|$ resulting in a large R. Further growth of ε_d leads to a decrease in the R factor as the difference between J_e^+ and $|J_e^-|$ becomes smaller and smaller (due to the growing similarity of Fermi-Dirac functions of both electrodes for high energies).

Interestingly, the rectification factor also grows when decreasing ε_d below $\varepsilon_d = \Delta$ reaching its maximal value for ε_d close to zero. Of course, for $\varepsilon_d = 0$ the thermocurrent vanishes due to particle-hole symmetry. However, even a small departure of the dot's energy level from zero results in an extremely small thermocurrent due to the difference in tail profiles of dot's level contributing to quasiparticle tunneling above Δ and below $-\Delta$. Although both J_e^+ and $|J_e^-|$ are extremely small, their ratio turns out to be large for $\varepsilon_d \approx 0$ and decreases with increasing dot's energy level up to $\varepsilon_d = \Delta$.

A similar analysis can be carried out for negative ε_d resulting in the same behavior of the rectification ratio R as shown above.

Finally, we introduce the nonlinear Seebeck coefficient (thermopower), the quantity which is more available in nanoscopic experiments and a subject of recent investigations [30–33]. The Seebeck coefficient is defined as;

$$S = -\left.\frac{V_{th}}{\delta T}\right|_{J_e=0} \tag{16}$$

the ratio of thermally generated bias voltage to the temperature difference within the condition of vanishing charge current. Note, that opposite to the linear response regime, here V_{th} and δT are finite. In Fig. 5 we show the non-equilibrium Seebeck coefficient as a function of the dot's energy level calculated for indicated temperature bias δT and for two values of the dot's coupling strength to the TS electrode, i. e. for symmetric case ($r = 1$) and highly asymmetric case ($r = 10$). One notices that the thermopower is strongly suppressed within the superconducting gap region, which results from the particle-hole symmetry. Indeed, for the particle-hole symmetry point, here $\varepsilon_d = 0$, the Seebeck coefficient is exactly zero as the current due to electrons is completely compensated by the current associated with the holes. Finite but vanishingly small thermopower in the superconducting gap region besides $\varepsilon_d = 0$ is due to the tail of the dot's level which contributes to quasiparticle transport. When the dot's energy level approaches the SC gap edge, the thermopower changes significantly. The positive value of S is associated with the fact that majority carriers are electrons, whereas the negative sign of the thermopower is because majority carriers are holes. The thermopower diminishes with decreasing temperature bias δT which is understood as the number of high energetic electrons in the NM lead decreasing and simultaneously the number of excited quasiparticles in the TS electrode being independent of the temperature bias. Moreover, the Seebeck coefficient drops with increasing coupling to the TS electrode. Apart from that, for larger coupling to the TS lead, finite thermopower leaks into the superconducting gap region.

4. Conclusions

In conclusion, we have studied out-of-equilibrium voltage and temperature bias response of a quantum dot system attached to topological superconductor and normal metal electrodes. Using Green's function techniques, we have determined the differential conductance, thermocurrent and the corresponding thermoconductance. We have shown the variation of these quantities when tuning the system's parameters. In particular, we have shown that, in general, the differential conductance consists of three sub-gap peaks and some above-gap features. Our results clearly state that the zero bias anomaly in the differential conductance, associated with Majorana bound state, is robust to changes in the dot's energy level. In turn, the remaining two side-peaks are very sensitive to variations of the dot's level position. Moreover, the above-gap features, corresponding to quasiparticle tunneling, become relevant as the dot's energy level is situated close to the SC gap or beyond it. Apart from that, we have analyzed in detail the temperature dependence of the differential conductance.

We have also investigated current generation by means of a temperature gradient applied to the external electrodes. It has been shown that thermocurrent and thermoconductance reveal striking differences in topological and normal phases. We have shown that thermally induced thermocurrent reveals strong asymmetry under temperature bias reversal which can lead to a rectifying effect. Interestingly, we have also indicated conditions under which the strong rectifying effect is present and the system can work as a diode. Moreover, we have also investigated the nonlinear Seebeck coefficient — a quantity that is more available in nanoscopic experiments than the thermoconductance.

CRediT authorship contribution statement

Piotr Trocha: Conceptualization, Data curation, Formal analysis, Funding acquisition, Methodology, Project administration, Software, Validation, Visualization, Writing – original draft, Writing – review & editing. **Thibaut Jonckheere:** Formal analysis, Funding acquisition, Supervision, Writing – review & editing. **Jérôme Rech:** Formal analysis, Funding acquisition, Supervision, Writing – review & editing. **Thierry Martin:** Conceptualization, Formal analysis, Funding acquisition, Supervision, Writing – review & editing.

Declaration of competing interest

The authors declare that they have no known competing financial interests or personal relationships that could have appeared to influence the work reported in this paper.

Data availability

Data will be made available on request.

Acknowledgments

This work received support from the French government under the France 2030 investment plan, as part of the Initiative d'Excellence d'Aix-Marseille Université - A*MIDEX, through the institutes IPhU (AMX-19-IET-008) and AMUtech (AMX-19-IET-01X). P T. acknowledges support of the National Science Center in Poland through the research Project No. 2018/31/D/ST3/03965.

References

[1] V. Mourik, K. Zuo, S.M. Frolov, S.R. Plissard, E.P.A.M. Bakkers, L.P. Kouwenhoven, Signatures of Majorana Fermions in hybrid superconductor-semiconductor nanowire devices, Science 336 (6084) (2012) 1003–1007, http://dx.doi.org/10.1126/science.1222360.

[2] M.T. Deng, C.L. Yu, G.Y. Huang, M. Larsson, P. Caroff, H.Q. Xu, Anomalous zero-bias conductance peak in a Nb–Insb nanowire–Nb hybrid device, Nano Lett. 12 (12) (2012) 6414–6419, http://dx.doi.org/10.1021/nl303758w.

[3] M.T. Deng, S. Vaitiekėnas, E.B. Hansen, J. Danon, M. Leijnse, K. Flensberg, J. Nygård, P. Krogstrup, C.M. Marcus, Majorana bound state in a coupled quantum-dot hybrid-nanowire system, Science 354 (6319) (2016) 1557–1562, http://dx.doi.org/10.1126/science.aaf3961.

[4] M. Leijnse, K. Flensberg, Scheme to measure Majorana fermion lifetimes using a quantum dot, Phys. Rev. B 84 (2011) 140501, http://dx.doi.org/10.1103/PhysRevB.84.140501.

[5] D.E. Liu, H.U. Baranger, Detecting a Majorana-fermion zero mode using a quantum dot, Phys. Rev. B 84 (2011) 201308, http://dx.doi.org/10.1103/PhysRevB.84.201308.

[6] R. López, M. Lee, L. Serra, J.S. Lim, Thermoelectrical detection of Majorana states, Phys. Rev. B 89 (2014) 205418, http://dx.doi.org/10.1103/PhysRevB.89.205418.

[7] M. Leijnse, Thermoelectric signatures of a Majorana bound state coupled to a quantum dot, New J. Phys. 16 (1) (2014) 015029, http://dx.doi.org/10.1088/1367-2630/16/1/015029.

[8] Y.-J. Zheng, J. Song, Y.-X. Li, Anomalous thermoelectric properties in double quantum dots coupled with Majorana bound states, AIP Adv. 6 (12) (2016) http://dx.doi.org/10.1063/1.4972261, 125032.

[9] L.S. Ricco, F.A. Dessotti, I.A. Shelykh, M.S. Figueira, A.C. Seridonio, Tuning of heat and charge transport by Majorana fermions, Sci. Rep. 8 (1) (2018) 2790, http://dx.doi.org/10.1038/s41598-018-21180-9.

[10] X.-Q. Wang, S.-F. Zhang, Y. Han, G.-Y. Yi, W.-J. Gong, Efficient enhancement of the thermoelectric effect due to the Majorana zero modes coupled to one quantum-dot system, Phys. Rev. B 99 (2019) 195424, http://dx.doi.org/10.1103/PhysRevB.99.195424.

[11] C.W. Ri, K.H. Jong, S.J. Im, H.C. Pak, Thermoelectric transport through a finite-u quantum dot side-coupled to Majorana bound state, Eur. Phys. J. B 92 (5) (2019) 90, http://dx.doi.org/10.1140/epjb/e2019-90593-0.

[12] L. Hong, F. Chi, Z.-G. Fu, Y.-F. Hou, Z. Wang, K.-M. Li, J. Liu, H. Yao, P. Zhang, Large enhancement of thermoelectric effect by Majorana bound states coupled to a quantum dot, J. Appl. Phys. 127 (12) (2020) http://dx.doi.org/10.1063/1.5125971, 124302.

[13] P.-B. Niu, L. Liu, X. Su, L. Dong, Y. Shi, H.-G. Luo, Spin seebeck effect induced by a Majorana zero mode in a nanomagnet, Physica E 124 (2020) 114313, http://dx.doi.org/10.1016/j.physe.2020.114313.

[14] G.A.R. van Dalum, A.K. Mitchell, L. Fritz, Wiedemann-franz law in a non-Fermi liquid and Majorana central charge: Thermoelectric transport in a two-channel Kondo system, Phys. Rev. B 102 (2020) 041111, http://dx.doi.org/10.1103/PhysRevB.102.041111.

[15] F. Chi, Z.-G. Fu, J. Liu, K.-M. Li, Z. Wang, P. Zhang, Thermoelectric effect in a correlated quantum dot side-coupled to Majorana bound states, Nanoscale Res. Lett. 15 (1) (2020) 79, http://dx.doi.org/10.1186/s11671-020-03307-y.

[16] S. Smirnov, Majorana entropy revival via tunneling phases, Phys. Rev. B 103 (2021) 075440, http://dx.doi.org/10.1103/PhysRevB.103.075440.

[17] L.-L. Sun, F. Chi, Detecting spin heat accumulation by sign reversion of thermopower in a quantum dot side-coupled to Majorana bound states, J. Low Temp. Phys. 203 (5) (2021) 381–391, http://dx.doi.org/10.1007/s10909-021-02593-9.

[18] P. Majek, K.P. Wójcik, I. Weymann, Spin-resolved thermal signatures of Majorana-Kondo interplay in double quantum dots, Phys. Rev. B 105 (2022) 075418, http://dx.doi.org/10.1103/PhysRevB.105.075418.

[19] I. Grosu, I. Tifrea, Thermoelectric transport properties of single quantum dot systems in the presence of Majorana states, Physica E 145 (2023) 115503, http://dx.doi.org/10.1016/j.physe.2022.115503.

[20] A.C.P. Lima, R.C.B. Ribeiro, J.H. Correa, F. Deus, M.S. Figueira, M.A. Continentino, Thermoelectric properties of topological chains coupled to a quantum dot, Sci. Rep. 13 (1) (2023) 1508, http://dx.doi.org/10.1038/s41598-023-28491-6.

[21] S. Valentini, R. Fazio, V. Giovannetti, F. Taddei, Thermopower of three-terminal topological superconducting systems, Phys. Rev. B 91 (2015) 045430, http://dx.doi.org/10.1103/PhysRevB.91.045430.

[22] A. Zazunov, R. Egger, A. Levy Yeyati, Low-energy theory of transport in Majorana wire junctions, Phys. Rev. B 94 (2016) 014502, http://dx.doi.org/10.1103/PhysRevB.94.014502.

[23] Z.Y. Zeng, B. Li, F. Claro, Electronic transport in hybrid mesoscopic structures: A nonequilibrium green function approach, Phys. Rev. B 68 (2003) 115319, http://dx.doi.org/10.1103/PhysRevB.68.115319.

[24] M. Tinkham, Introduction to Superconductivity, second ed., Dover Publications, 2004.

[25] S. Verma, A. Singh, Non-equilibrium thermoelectric transport across normal metal–quantum dot–superconductor hybrid system within the Coulomb blockade regime, J. Phys.: Condens. Matter 34 (15) (2022) 155601, http://dx.doi.org/10.1088/1361-648X/ac4ced.

[26] P. Trocha, J. Barnaś, Spin-polarized Andreev transport influenced by Coulomb repulsion through a two-quantum-dot system, Phys. Rev. B 89 (2014) 245418, http://dx.doi.org/10.1103/PhysRevB.89.245418.

[27] P. Trocha, J. Barnaś, Spin-dependent thermoelectric phenomena in a quantum dot attached to ferromagnetic and superconducting electrodes, Phys. Rev. B 95 (2017) 165439, http://dx.doi.org/10.1103/PhysRevB.95.165439.

[28] A.A. Aligia, D.P. Daroca, L. Arrachea, P. Roura-Bas, Heat current across a capacitively coupled double quantum dot, Phys. Rev. B 101 (2020) 075417, http://dx.doi.org/10.1103/PhysRevB.101.075417.

[29] G.T. Craven, D. He, A. Nitzan, Electron-transfer-induced thermal and thermoelectric rectification, Phys. Rev. Lett. 121 (2018) 247704, http://dx.doi.org/10.1103/PhysRevLett.121.247704.

[30] L. Rincón-García, C. Evangeli, G. Rubio-Bollinger, N. Agraït, Thermopower measurements in molecular junctions, Chem. Soc. Rev. 45 (2016) 4285–4306, http://dx.doi.org/10.1039/C6CS00141F.

[31] A. Dorda, M. Ganahl, S. Andergassen, W. von der Linden, E. Arrigoni, Thermoelectric response of a correlated impurity in the nonequilibrium Kondo regime, Phys. Rev. B 94 (2016) 245125, http://dx.doi.org/10.1103/PhysRevB.94.245125.

[32] P.A. Erdman, F. Mazza, R. Bosisio, G. Benenti, R. Fazio, F. Taddei, Thermoelectric properties of an interacting quantum dot based heat engine, Phys. Rev. B 95 (2017) 245432, http://dx.doi.org/10.1103/PhysRevB.95.245432.

[33] B. Dutta, D. Majidi, A. García Corral, P.A. Erdman, S. Florens, T.A. Costi, H. Courtois, C.B. Winkelmann, Direct probe of the seebeck coefficient in a Kondo-correlated single-quantum-dot transistor, Nano Lett. 19 (1) (2019) 506–511, http://dx.doi.org/10.1021/acs.nanolett.8b04398.